Analytica Chimica Acta 1228 (2022) 340299

Contents lists available at ScienceDirect

Analytica Chimica Acta

journal homepage: www.elsevier.com/locate/aca

An entropy-driven three-dimensional multipedal-DNA walker for ultrasensitive detection of cancer cells

Hong Jiang [a,b], Li-Bin Wang [a], Ya-Ting Zhang [a], Min Dong [a], Jian Li [a], Ji-Dong Wang [a,b,*]

[a] Nano-biotechnology Key Lab of Hebei Province, Hebei Key Laboratory of Applied Chemistry, College of Environmental and Chemical Engineering, Yanshan University, Qinhuangdao, 066004, China
[b] State Key Laboratory of Metastable Materials Science and Technology, Yanshan University, Qinhuangdao, 066004, China

HIGHLIGHTS

- Cancer cells detection by entropy-driven DNA walker.
- Bipedal hairpin fuel chain combines with the rolling of DTNs to achieve multipedal walking of DNA walkers.
- 3D multipedal-DNA walker increases the reaction rates and sensitivity of entropy-driven DNA walker.

GRAPHICAL ABSTRACT

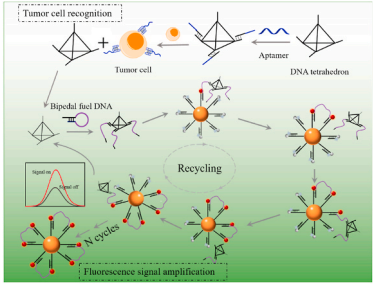

ARTICLE INFO

Keywords:
Entropy-driven
Multipedal-DNA walker
3D track
Signal amplification strategy
Cancer cells detection

ABSTRACT

Sensitive and accurate detection of cancer cells is of great significance for the early diagnosis and treatment of cancer. In this work, we developed a simple fluorescent signal amplification biosensor based on an entropy-driven three-dimensional (3D) multipedal-DNA walker for highly sensitive detection of cancer cells. Firstly, DNA tetrahedron nanostructures (DTNs) combined with AS1411 aptamer were used as the capture probe to achieve efficient capture of cancer cells. Then, the bipedal hairpin fuel chain hybridized with DTNs and exposed two catalytic "legs" to form a walker probe. Finally, the walker probe autonomously walked on polystyrene microspheres (PS) via entropy-driven catalytic reaction. DTNs rolled on the PS to achieve multipedal walking, realizing fluorescence signal amplification due to fluorescence recovery of DNA-CdTe quantum dots on the PS surface. This fluorescence signal amplification strategy showed excellent selectivity and sensitivity toward cancer cells with the detection limit of 7 cell mL^{-1}. This entropy-driven 3D multipedal DNA walker fluorescence exhibited great potential in detecting circulating tumor cells and tumor markers used for early diagnosis and clinical treatment of cancer.

* Corresponding author. Nano-biotechnology Key Lab of Hebei Province, Hebei Key Laboratory of Applied Chemistry, College of Environmental and Chemical Engineering, Yanshan University, Qinhuangdao, 066004, China.
E-mail address: jidongwang1975@sina.com (J.-D. Wang).

https://doi.org/10.1016/j.aca.2022.340299
Received 11 May 2022; Received in revised form 18 August 2022; Accepted 18 August 2022
Available online 27 August 2022

1. Introduction

Cancer, one of the most severe diseases globally, remains the main cause of human death so far [1,2]. Developing an accurate and sensitive cancer cells detection strategy has been of great importance for diagnosing and treating cancer. Currently, a series of technologies based on polymerase chain reaction (PCR) [3,4], flow cytometry [5,6], immunohistochemistry [7,8], and mass spectrometry [9] have been developed for detecting cancer cells. However, most of these methods are restricted by their time-consuming procedures, complicated platform, high cost, and poor stability. In particular, for the lack of an efficient signal amplification strategy, these methods exhibit a limited sensitivity for detecting cancer cells due to their low concentration at early stages and heterogeneity.

As a powerful DNA nanomachine, the DNA walkers have been developed and applied in biosensing and biological imaging due to its predictable properties, selectivity, and accurate Watson-Crick base pairing. So far, DNA walker have been used in sensing detection of DNA [10,11], miRNA [12–14], protein [15,16], mycotoxin [17], etc. Entropy-driven DNA walkers are an enzyme-free DNA nanomachine first presented by Zhang et al., in 2007, which utilizes single-stranded linear DNA molecules to activate a sequence of DNA hybridization and dissociation reactions to achieve a signal amplification [18]. Due to the absence of enzymes, the entropy-driven DNA walkers exhibit excellent stability in different environmental conditions, such as temperature, pH, and salt concentrations. Moreover, because the complicated second structure in DNA is absent, the background signal is significantly reduced in entropy-driven DNA walkers to avoid undesired interaction between metastable hairpin structures [19,20]. However, some drawbacks, such as relatively slow reaction rates in solution, and lower sensitivity, limit entropy-driven DNA walker in sensing the low-level targets [21]. Three-dimensional (3D) DNA walkers, which move continuously and controllably on the 3D surface of micro- or nanoparticles, possess better sensitivity than the 2D surface due to their strong loading capability and broader moving space. Jung et al. developed a 3D DNA walker that used catalytic hairpin assembly to drive walking on DNA-coated microparticle surfaces, and the walker could take more than 30 continuous steps [22]. Cheng et al. reported a flap endonuclease 1-assisted 3D DNA walker system to detect DNA target and mutation abundance, and the theoretical detection limits were down to 0.22 fM and 0.01%, respectively [23]. Although the detection sensitivity was improved via the 3D DNA walker, the walking steps with one leg were not enough for the high-efficiency sensing detection. Recently, multipedal DNA walkers have gained extensive attention because they can accelerate the walking reaction and enhance amplification efficiency. Lv et al. reported a bipedal DNA walker that autonomously traveled on gold nanoparticles via the catalytic hairpin assembly reaction, resulting in the amplified fluorescence signal for highly sensitive detection of low-abundance biomarker APE1 activity inside living cells. Meanwhile, they demonstrated that the bipedal DNA walker showed excellent kinetics and walking steps [24]. Xiong et al. proposed a cascade signal amplification biosensing platform based on a protein binding-induced 3D-bipedal DNA walker to detect thrombin. The detection limit was as low as 23 fM [25]. Although various multipedal DNA walkers have been developed, complex chemical modification and multiple assembly processes of DNA legs are tedious. Moreover, multipedal DNA walkers are rarely found in detecting cancer cells directly or indirectly because achieving efficient capture of cancer cells and preventing the signal probe from endocytosis of cells remains challenging.

Hence, an entropy-driven 3D multipedal-DNA walker fluorescent signal amplification strategy for ultrasensitive sensing detection for cancer cells was reported. As Scheme 1 depicted, the process of this entropy-driven 3D multipedal DNA walker involved two parts: the construction of the multipedal DNA walker probe and the 3D movement track by catalytic recycling. In the first part, to construct the multipedal DNA walker probe, DNA tetrahedron nanostructures (DTNs) with single-stranded DNA pendants (the sequence of the target strand) at three vertices were synthesized. And then, the aptamer AS1411 was assembled on the single-stranded DNA pendant of DTNs to form the capture probe (DTNs-AS1411). When HeLa cells were presented as model targets, DTNs-AS1411 would interact with nucleolin on the surface of the cell membrane, which exhibited excellent resistance to the endocytosis

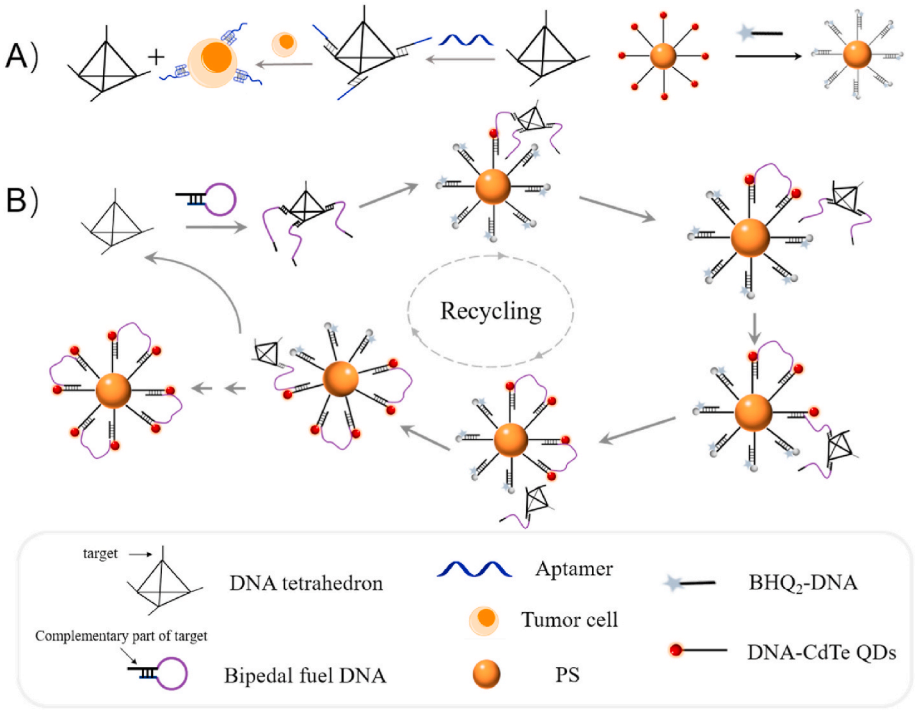

Scheme 1. Schematic illustration of the fluorescence signal amplification via the entropy-driven 3D multipedal DNA walker strategy. A) The process of cancer cell recognition. B) The process of fluorescence signal amplification.

of cells under optimized incubation time [26]. In the meantime, AS1411 would dissociate from the capture probe due to its structure evolution to stable dimeric G-quadruplex on membranes of cancer cells [27,28], accompanied by the release of DTNs and the exposure of the target sequence on the pendant. Subsequently, the exposed "target" strand on the DTNs hybridized with bipedal hairpin fuel chain (F2) and triggered the opening of F2 to expose two catalytic "legs" to form the walker probe (Fig. S1). In the second part, to construct the 3D movement track, the synthesized 5′–NH_2–ssDNA (denoted as "S" strand) functionalized CdTe quantum dots (DNA-CdTe QDs), whose excitation and emission wavelengths were 365 nm and 597 nm, respectively, bond to the surface of COOH-polystyrene microspheres (COOH-PS). Meanwhile, a complementary DNA sequence with BHQ2 (denoted as "Q" strand) hybridized with S strand, leading to fluorescence quenching of DNA-CdTe QDs under light irradiation of 365 nm due to the fluorescence resonance energy transfer (FRET) between the DNA-CdTe QDs and quencher (BHQ2). Therefore, 3D walking track and fluorescent signal probe were obtained. Finally, the two catalytic "legs" of walker probe alternately hybridized with the S and autonomously traveled on PS via entropy-driven catalytic reaction, resulting in separation between the DNA-CdTe QDs and BHQ2 and fluorescence recovery of DNA-CdTe QDs. Meanwhile, DTNs could roll on the PS to achieve a multipedal walking, realizing fluorescence signal amplification. The multipedal entropy-driven 3D DNA walker showed excellent stability, selectivity, and capabilities of signal amplification, and realized the highly sensitive detection of HeLa cells, which provided a simple and high-efficiency signal amplification strategy for highly sensitive detection of cancer cells.

2. Experimental section

2.1. Synthesis of DNA-CdTe QDs

The DNA-CdTe QDs were synthesized as previously reported [29,30]. Briefly, the $CdCl_2$ (1.2 mmol) and 3-mercaptopropionic acid (1.2 mmol) were added to 25 ml of deionized water under vigorous stirring, and the pH of the mixture solution was adjusted to 10.5. Then, Na_2TeO_3 (0.15 mmol) and $NaBH_4$ (3 mmol) were added to the above mixture solution.

According to the previous work, the fluorescence emission wavelength of DNA-CdTe QDs exhibited a red shift with the increase of the reaction time [30]. The fluorescence intensity reached the maximum when the reaction time is 60 min. Therefore, to obtain the maximum fluorescence intensity of PS@S, 10 μL 5′–NH_2–ssDNA (10 μM) was added to 990 μL above mixture solution and heated to 90 °C for 60 min. Then, the DNA-CdTe QDs (denoted as "S" strand) solutions were washed with ethanol and distilled water three times.

In order to optimize the incubation time of DTNs and HeLa cells, 10 μL ssDNA C (10 μM) was added to 990 μL above mixture solution and heated to 90 °C for 45 min to obtain the C-QDs. The final DNA-CdTe QDs solution was also washed with ethanol and distilled water three times and then stored in the dark at 4 °C.

2.2. Synthesis of DNA tetrahedron probe (DTNs) and DTNs-CdTe QDs

To construct the DTNs, strand A, B, C, and D of the same concentration (10 μM) and volume (5 μL) were mixed in PBS buffer. Then, to construct DTNs-AS1411, we added excess AS1411 aptamer (10 μM, 20 μL) to the above solution, and the mixture solution was heated to 95 °C for 5 min. Finally, the mixture solution was cooled to room temperature, and washed with PBS buffer three times for various tests after 2 h. To construct the DTNs-CdTe QDs, the strand C in the above DTNs structure was replaced by C-QDs.

2.3. Synthesis of PS@S and PS@S-Q

20 μL carboxyl polystyrene microspheres (PS–COOH, 50 mg/mL) were washed three times by PBS buffer solution and suspended into 1 ml PBS buffer solution. Then, the 18 mg EDC and 27 mg NHS were added to the above solutions at 37 °C for 15 min to activate the PS-COOH. In order to obtain the optimal fluorescence signal of PS@S, a series of different volumes (10, 20, 30, 40, and 50 μL, respectively) S strand solutions (10 μM) were added to the above solutions to incubate 8 h at 37 °C. Then, the fluorescence intensity was monitored by an F-7000 fluorescence spectrophotometer. To obtain PS@S-Q, 2 μL ssDNA-BHQ2 was added to 100 μL PS@S (the volume of S is 30 μL) and incubated 8 h at room temperature.

2.4. Cells fluorescence imaging

To optimize the incubation time of DTNs-AS1411 and HeLa cells, the C-QDs and Cy5-AS1411 were chosen to fabricate the DNA tetrahedron capture probe (DTNs-QDs-AS1411-Cy5). As the control experiment, C-QDs were chosen to hybridize with Cy5-AS1411 to obtain C-QDs-Cy5-AS1411. The HeLa cells were seeded in a 35 mm Petri dish with a 1 mL culture medium at 37 °C for 24 h. Then, the cells were incubated with 100 μL DTNs-QDs-AS1411-Cy5 or C-QDs-Cy5-AS1411 (10 μM) for 15, 30, 45, and 60 min, respectively. After washing three times with PBS to remove DTNs-QDs-AS1411-Cy5 or C-QDs-Cy5-AS1411, which did not react with cells, the fluorescence microphotographs were taken by XSP-63X fluorescence microscope.

2.5. Cells experiment

Firstly, 50 μL PS@S-Q (10 μM) and 10 μL F2 (10 μM) were added to 500 μL PBS solutions to obtain 3D walker solutions. Then, the HeLa cells with different densities were incubated with 100 μL DTNs-AS1411 (10 μM) for 45 min, and then the suspension was centrifuged at 1000 rpm for 10 min. Finally, the 20 μL supernatant was incubated with the above 3D DNA walker solutions for 45 min, and the fluorescence intensity was recorded by an F-7000 (Hitachi, Tokyo, Japan).

3. Results and discussion

3.1. Characterization of DNA tetrahedron nanostructure

To improve the recognition ability and signal amplification efficiency of the capture probe, DTNs were designed in which three single-stranded DNA pendants were at vertices, serving as the hybridizing with AS1411 to construct the capture probe and triggering the opening of the bipedal hairpin fuel chain (F2) to form DNA walker probe. To ensure that the target sequence on the DTN pendant is fully bonded to AS1411, we added excess AS1411 aptamer to the DTNs solution. Moreover, the other vertex had a phosphorothioate linkage that served as a ligand structure for the synthesis of QDs. The successful formation of DTNs was first verified by agarose gel electrophoretic experiments. As shown in Fig. 1A, strand A, A + B, A + B + C, A + B + C + D, and A + B + C + D + AS1411 were exhibited in Lane 1–5, respectively. The gel electrophoresis analysis demonstrated the successful assembly of DTNs as Line 4 because the band of a combination containing four ssDNA moved more slowly than other bands. There was no significant difference in the mobility of Lane 4 and 5 after AS1411 was assembled on DTNs because it is only a short-chain. Moreover, the AFM and TEM image showed the average height and size was about 6.9 ± 0.6 nm and 6.8 ± 0.5 nm in the dried state, which was a bit larger than the calculated height of the DTNs (The four sides of DTNs consist of 17 base pairs. Therefore, the height of DTN is about 6 nm due to the distance between each base pair is 0.34 nm) due to the presence of AS1411 (Fig. S2).

Due to the polyanionic nature of DNA, DTNs usually be considered as nanoparticles and easy to be intracellular uptake without transfection

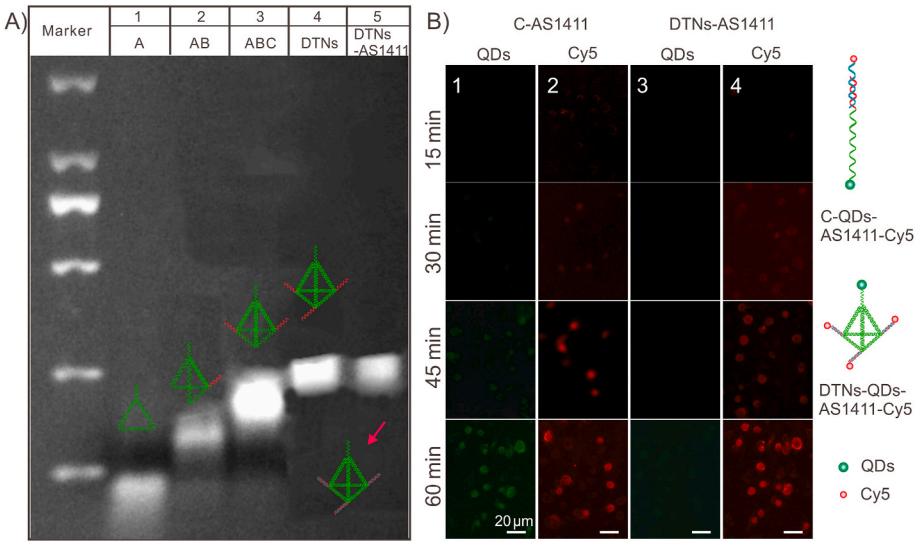

Fig. 1. A) Agarose gel electrophoresis of the fold DNA nanostructure. Lane 1: A strand; Lane 2: A + B; Lane 3: A + B + C; Lane 4: A + B + C + D; Lane 5: A + B + C + D + AS1411. B) Fluorescence images of HeLa cells incubated with C-QDs-AS1411-Cy5 or DTNs-QDs-AS1411-Cy5 for 15, 30, 45, and 60 min, respectively.

agents [31]. As we know, the endocytosis of DTN is a time-dependent process. To balance cell recognition and cell-endocytosis event, incubate time of single-strand DNA (ssDNA) and DTNs with HeLa cell were investigated, as shown in Fig. 1B. A hybrid DNA template, strand C, was designed containing a phosphorothioate domain at the 5' end for the growth of the CdTe QDs and two phosphate domains for the assembly of DTNs and hybridization of aptamer AS1411. Strand C functionalized CdTe QDs (C-QDs) were synthesized via a one-pot route as in our previous work [29,30]. The TEM image and the particle size distribution histogram showed that the diameter of C-QDs was about 2.5 nm (Fig. S3). The emission wavelength was 570 nm under an excitation wavelength of 365 nm when reaction time was 45 min (Fig. S4). C-QDs-AS1411-Cy5 and DTNs-QDs-AS1411-Cy5 described in Fig. 1B were obtained through assembled Cy5-labeled-aptamer AS1411 coupled with C-QDs and C-QDs assembled DTNs. We discussed the interaction between the HeLa cells and AS1411-Cy5 and DTNs-QDs-AS1411-Cy5 by distinguishing color. The fluorescence of CdTe QDs and Cy5 exhibited green and red colors under an excitation wavelength of 365 nm and 650 nm. C-QDs-AS1411-Cy5 and DTNs-QDs-AS1411-Cy5 were incubated with HeLa cells for 15 min, 30 min, 45 min, and 60 min, respectively. As shown in Fig. 1B, Cy5 fluorescence (red) in C-QDs-AS1411-Cy5 and DTNs-QDs-AS1411-Cy5 were observed after 30 min, which indicated that the AS1411 interacted with nucleolin on the surface of the HeLa cell. The QDs fluorescence (green) in C-QDs-AS1411-Cy5 was observed after 30 min, while a weak fluorescence of QDs in DTNs-QDs-AS1411-Cy5 was shown after 60 min, which demonstrated that the ssDNA began to be endocytosed after 30min and the endocytosis of DTNs appeared after 60 min. These results showed that the modification of ssDNA with AS1411 aptamer increased its endocytosis by cells and solved the problem of poor permeability of ssDNA, which is consistent with the previously reported [32,33]. These results indicated that the DTNs were more suitable as a capture probe than ssDNA for the subsequent signal amplification process. The optimal incubating time of DTNs with cancer cells was less than 45 min.

3.2. Characterization of the 3D tracks

Three-dimensional (3D) DNA walkers walking along the surface of nano-/micro-particles have drawn particular attention due to their larger surface area, high mobility, and powerful carrying capacity. Herein, COOH-PS with a diameter of 1 μm was chosen to construct 3D walking tracks, and NH_2-ssDNA S functionalized CdTe QDs bond to the surface of PS (PS@S) through amide bonds. After then optimized the incubation time and concentration of PS and S strand, and the optimal incubation time was 8 h (Fig. S5). The optimal fluorescence intensity could be obtained by adding a 0.3 nmol S strand to 20 μL PS solutions (Fig. S6). Compared with the very smooth surface of the PS (Fig. 2A), some synapses were distributed on the PS surface (Fig. 2B), and the results of large-scale TEM images were consistent with the above results (Fig. S7), which also indicated that CdTe QDs were linked on the PS. Moreover, both Cd, Te, N, P, and S elements in SEM-EDX mapping (Fig. 2C), and red fluorescence of CdTe QDs in fluorescence images (Fig. S8), also demonstrated that S strand functionalized CdTe QDs had grafted on the surface of COOH-PS. Then, the ssDNA-BHQ2 was chosen as the quencher of QDs and hybridized with S strand, which had a linker on the surface of PS. Due to the absorption spectrum of the BHQ2 overlaps well with the emission spectrum of the CdTe QDs (Fig. 2D), it provided an efficient FRET process between QDs and BHQ2. As observed in Fig. 2E, after the strand Q hybridized with strand S, the fluorescence intensity of QDs was quenched by 62%. Therefore, 3D DNA walking tracks were achieved.

3.3. Feasibility of the entropy-driven bipedal DNA walker

We used a single strand "target" as the initiator to verify the feasibility of the 3D entropy-driven DNA walker in solutions. The agarose gel electrophoresis results were shown in Fig. 3A. Lane 1 and 2 represented the target strand and F2, respectively. Compared with Lane 1 and Lane 2, a new band appeared in Lane 3 (the mixture of target strand and F2), which indicated the "target" strand hybridized with complementary sequences on F2 and triggered the opening of F2. The new band with higher molecular weight in Lane 4 suggested that the mixture of S and Q strand hybridized to form a stable complex. Compared with bands in Lane 1 and Lane 4, the mixture of S-Q and target strand in Lane 5 could coexist stably in the solution without F2. Similarly, the mixture of S-Q and F2 could coexist without the target. In the presence of the target, the mixture of S-Q and F2, target bands (Lane 1), and two new bands different from Lane 3 and 4 appeared, which indicated the entropy-driven DNA walker was successfully initiated by the target (Fig. 3B). In addition, we adopted fluorescence spectrometry to prove the signal amplification process of the entropy-driven DNA walker (Fig. 3C). The fluorescence signal of S strand was quenched when the presence of Q strand. When the F2 was added to S-Q, no obvious fluorescence enhancement was observed. However, in the presence of the target, the

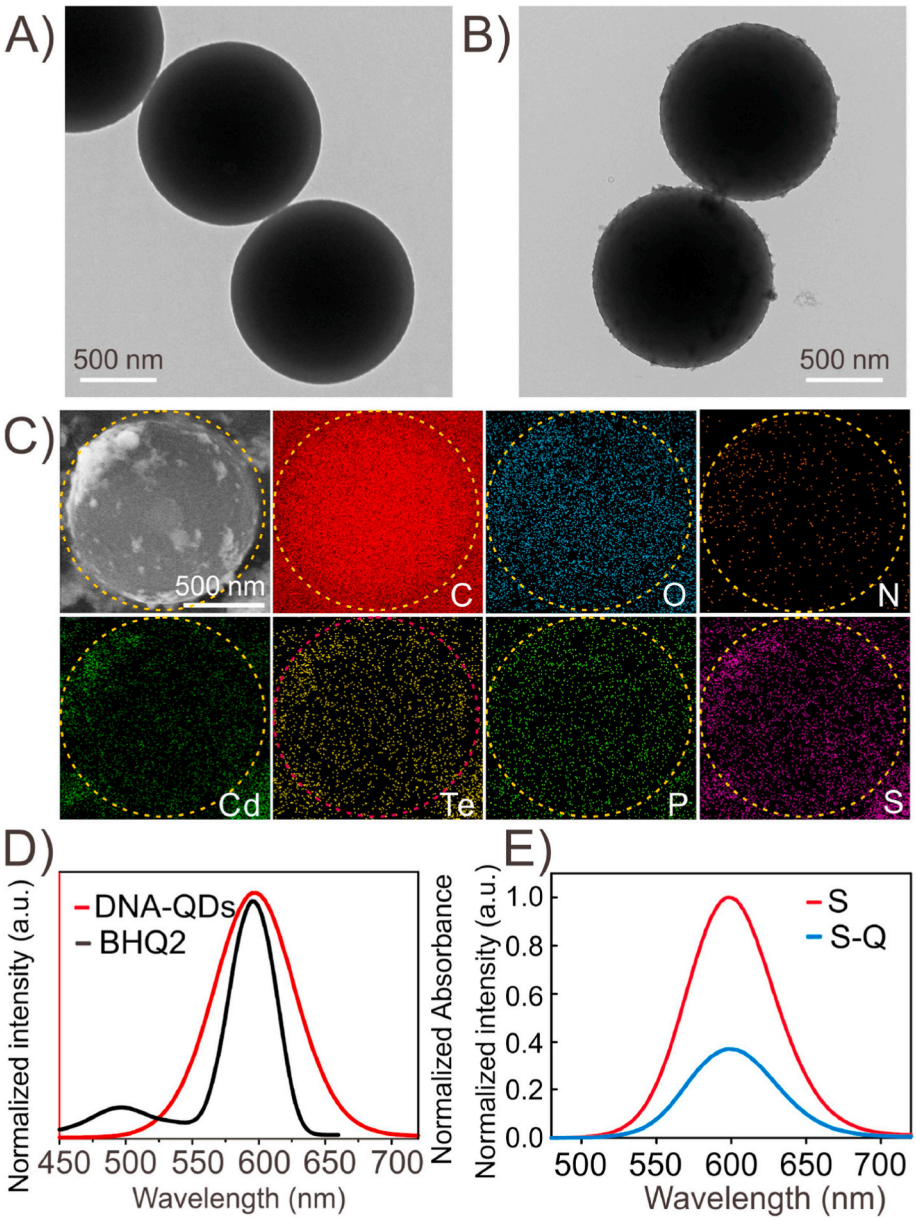

Fig. 2. Characterization of PS@S. A) TEM images of PS and PS@S B). C) SEM image of PS@S and corresponding EDX elemental mapping images of C, O, N, Cd, Te, P, and S. D) The fluorescence emission spectra of strand S (red) and the absorption spectra of strand Q. E) Fluorescence spectrometry of strand S and S-Q. (For interpretation of the references to color in this figure legend, the reader is referred to the Web version of this article.)

fluorescence intensity recovered to 85.5% when F2 was added to S-Q. These results demonstrated that when the presence of the target strand, the entropy-driven DNA walker could achieve fluorescence signal amplification. Furthermore, we found the optimal value of fluorescence intensity at pH 7.4 (Fig. S9), which meant that the entropy-driven DNA walker could perform in the physiological environment. The stability test showed that the S-Q complex structure kept stable within 100 h (Fig. S10). Simultaneously, we employed the unipedal hairpin fuel chain (F1) instead of F2 to conduct the above agarose gel electrophoresis experiment (Fig. S11). The experimental results we obtained were the same as Fig. 3A, which indicated that F1 could also trigger the entropy-driven DNA walker. However, fluorescence spectrometry showed when the F1 was added to S-Q + target, the fluorescence intensity recovered to 67.5%, which was 18% lower than F2. Moreover, the kinetic analysis showed that the bipedal hairpin fuel chain displayed faster velocity than that of the unipedal hairpin fuel chain (Fig. S12). These results confirmed that the entropy-driven multipedal DNA walker exhibited better kinetics and higher fluorescence signal amplification.

3.4. Cell detection

Based on the above investigations, we next tested the detecting ability of cancer cells by this strategy of the entropy-driven multipedal 3D DNA walker. HeLa cells with different concentrations were pre-incubated with DTNs-AS1411 for 45 min and then centrifuged to collect the supernatant. And then, the isolated DTNs were added to DNA walker solutions. As shown in Fig. 4A, the recovered fluorescence intensity was responded to the amount of HeLa cells, and the fluorescence intensity recovery showed a good linear relationship with the logarithm of HeLa cells concentration in the range from 1×10^2 to 1×10^6 cells mL^{-1} (Fig. 4B). The linear regression equation was, $(F- F_0)/(F_0) = -0.223 + 0.555$ lgC (C, cells mL^{-1}) with a correlation coefficient of 0.997 (n = 6). The limit of detection (LOD) was estimated to be 7 cells mL^{-1} (S/N = 3), which is lower than related methods (Table S2). In

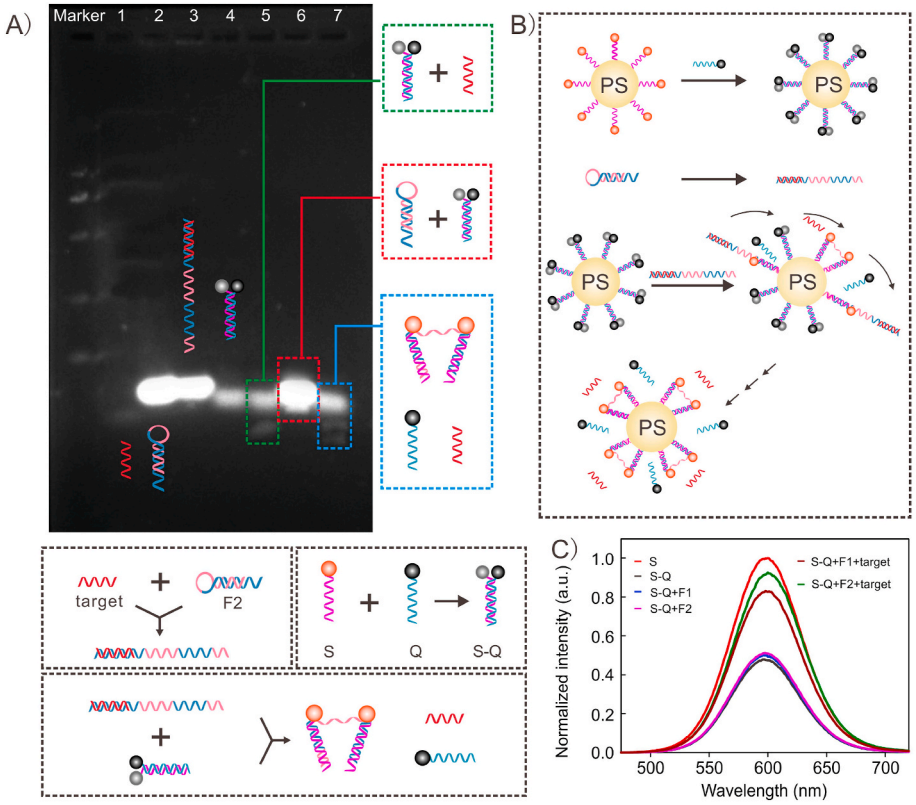

Fig. 3. A) Agarose gel electrophoresis of entropy-driven multipedal catalytic reactions. Lane 1, target; Lane 2, F2 (bipedal fuel); Lane 3, the mixture of target and F2; Lane 4, the mixture of S strand and Q strand; Lane 5, the mixture of S strand, Q strand and target; Lane 6, the mixture of S strand, Q strand, and F2; Lane 7, the mixture of the target, F2, S strand and Q strand. B) Schematic diagrams represent of the process of entropy-driven DNA walker for target analysis in solutions. C) The fluorescence spectrometry of the mixtures, S strand (red line), S-Q (black line), S-Q and F1 (unipedal fuel, blue line), S-Q and F2 (pink line), S-Q, F1, and target strand (brown line), S-Q, F2 and target strand (green line). (For interpretation of the references to color in this figure legend, the reader is referred to the Web version of this article.)

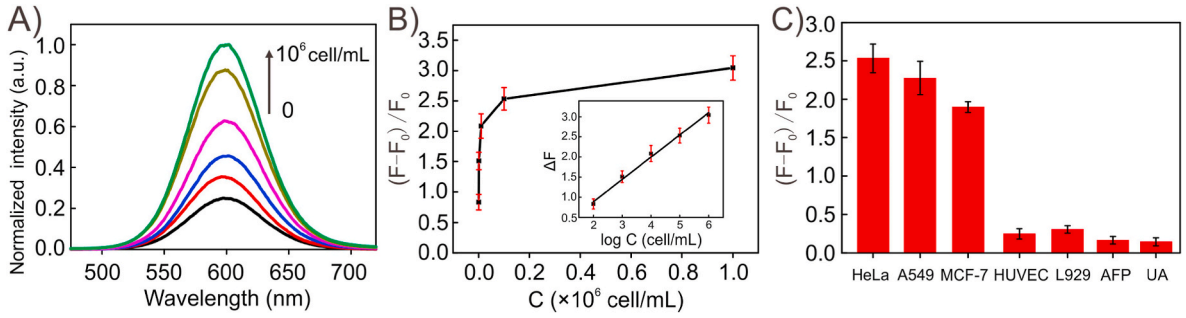

Fig. 4. A) Fluorescence spectrometry in the presence of HeLa cells at different concentrations (from 0 to 10^6 cell/mL) by the 3D multipedal-DNA walker. B) Relative fluorescence intensity ($(F - F_0)/F_0$) of the 3D multipedal-DNA walker in response to varying concentrations of HeLa cells. Inset shows the linear range. C) Selectivity assay of 3D multipedal-DNA walker towards cancer cells (A549 and MCF-7), normal cells (HUVEC and L929), and biomarkers (AFP and UA).

order to evaluate the selectivity of the entropy-driven 3D DNA walker, cancer cells (A549 and MCF-7, 10^5 cell/mL), normal cells (HUVEC and L929, 10^6 cell/mL), alpha-fetoprotein (AFP, 1 μg/mL), and uric acid (UA, 100 μg/mL) were investigated under identical conditions as HeLa cells (10^5 cell/mL). As shown in Fig. 4C, the fluorescence intensity recovered only when cancer cells were presented. However, normal cells and biomolecules (AFP and UA) would not interfere with the recognition of AS1411 for nucleolin on the surface of tumor cells, even if the concentration of normal cells is higher than that of cancer cells. These results demonstrated that the entropy-driven DNA walker could achieve fluorescence signal amplification in detecting cancer cells with high expression of nucleolin.

4. Conclusions

In summary, a versatile fluorescent signal amplification biosensor based on 3D multipedal entropy-driven DNA walker for cancer cell detection was developed. The DTNs-AS1411 composite was used as the capture probe to prevent DTNs from being endocytosed by cells, realizing efficient capture of cancer cells. The bipedal hairpin fuel chain walked on the PS via entropy-driven catalytic reaction, and DTNs could roll on the PS to achieve multipedal walking, achieving the fluorescence signal amplification. Compared to the unipedal hairpin fuel chain, the bipedal hairpin fuel chain provided excellent kinetics and higher fluorescence signal amplification. Combining the high specific recognition of AS1411, the high-efficiency reaction of bipedal hairpin fuel chain, high-capacity of 3D traces on PS, and the high photo-stability of quantum yields of QDs, we had achieved a selective capture and highly sensitive sensing detection for cancer cells based on fluorescent signal amplification strategy of entropy-driven 3D multipedal-DNA walker. The entropy-driven 3D multipedal-DNA walker displayed good selectivity, stability, and wide linear range (1×10^2 to 1×10^6 cells mL^{-1}), and the low LOD (7 cells mL^{-1}). This DNA nanomachine-assisted signal amplification method could be further used to detect circulating tumor cells and other biomarkers of cancer cells by the corresponding aptamer, holding great potential in early diagnosis and clinical treatment.

CRediT authorship contribution statement

Hong Jiang: Methodology, Formal analysis, Writing – original draft. **Li-Bin Wang:** Methodology, Investigation, Visualization. **Ya-Ting Zhang:** Formal analysis, Visualization. **Min Dong:** Formal analysis, Visualization. **Jian Li:** Writing – review & editing. **Ji-Dong Wang:** Supervision, Conceptualization, Writing – review & editing, Funding acquisition.

Declaration of competing interest

The authors declare that they have no known competing financial interests or personal relationships that could have appeared to influence the work reported in this paper.

Data availability

Data will be made available on request.

Acknowledgment

This work was supported by the National Natural Science Foundation of China (No. 62071413), the Hebei Natural Science Foundation (No. F2020203056, C2019203556), the Hebei education department key project (No. ZD2020147).

Appendix A. Supplementary data

Supplementary data to this article can be found online at https://doi.org/10.1016/j.aca.2022.340299.

References

[1] F. Bray, I. Ferlay, I. Soerjomataram, R.L. Siegel, L.A. Torre, A. Jemal, Global cancer statistics 2018: globocan estimates of incidence and mortality worldwide for 36 cancers in 185 countries, CA A Cancer J. Clin. 68 (2018) 394–424.
[2] T. Vos, R.M. Barber, et al., Global, regional, and national incidence, prevalence, and years lived with disability for 301 acute and chronic diseases and injuries in 188 countries, 1990-2013: a systematic analysis for the Global Burden of Disease Study 2013, Lancet 386 (2015) 743–800.
[3] J. Tang, X.X. He, Y.L. Lei, H. Shi, Q.P. Guo, J.B. Liu, D.G. He, L.A. Yan, K.M. Wang, Temperature-responsive split aptamers coupled with polymerase chain reaction for label-free and sensitive detection of cancer cells, Chem. Commun. 53 (2017) 11889–11892.
[4] J.Z. Song, F.T. Lv, G.M. Yang, L.B. Liu, Q. Yang, S. Wang, Aptamer-based polymerase chain reaction for ultrasensitive cell detection, Chem. Commun. 48 (2012) 7465–7467.
[5] M.C. Estévez, M.B. O'Donoghue, X.L. Chen, W.H. Tan, Highly fluorescent dye-doped silica nanoparticles increase flow cytometry sensitivity for cancer cell monitoring, Nano Res. 2 (2009) 448–461.
[6] M. Helou, M. Reisbeck, S.F. Tedde, L.K. Richter, L. Bar, J.J. Bosch, R.H. Stauber, E. Quandt, O. Hayden, Time-of-flight magnetic flow cytometry in whole blood with integrated sample preparation, Lab Chip 13 (2013) 1035–1038.
[7] W.C.C. Tan, S.N. Nerurkar, H.Y. Cai, H.H.M. Ng, D.D. Wu, Y.T.F. Wee, J.C.T. Lim, J. Yeong, T.K.H. Lim, Overview of multiplex immunohistochemistry/immunofluorescence techniques in the era of cancer immunotherapy, Cancer Commun. 40 (2020) 135–153.
[8] S.K. Singh, C. Hawkins, L.D. Clarke, J.A. Squire, J. Bayani, T. Hide, R. M. Henkelman, M.D. Cusimano, P.B. Dirks, Identification of human brain tumor initiating cells, Nature 432 (2004) 396–401.
[9] Y. He, S.L. Chen, L. Huang, Z.W. Wang, Y.N. Wu, F.F. Fu, Combination of magnetic-beads-based multiple metal nanoparticles labeling with hybridization chain reaction amplification for simultaneous detection of multiple cancer cells with inductively coupled plasma mass spectrometry, Anal. Chem. 91 (2019) 1171–1177.
[10] Q.Q. Cai, D. Wu, H.K. Li, G.F. Jie, H. Zhou, Versatile photoelectrochemical and electrochemiluminescence biosensor based on 3D CdSe QDs-DNA nanonetwork-SnO_2 nanoflower coupled with DNA walker amplification for HIV detection, Biosens. Bioelectron. 191 (2021), 113455.
[11] C.G. Feng, C. Zhang, J.X. Guo, G.P. Li, B.X. Ye, L. Zou, Novel preparation method of bipedal DNA walker based on hybridization chain reaction for ultrasensitive DNA biosensing, Anal. Chim. Acta 1176 (2021), 338781.
[12] P. Miao, Y. Tang, DNA walking and rolling nanomachine for electrochemical detection of miRNA, Small 16 (2020), 2004518.
[13] L. Yang, J. Fang, J.J. Lin, X.Y. Ou, L. Zhang, Y.F. Wang, Z. Weng, G.M. Xie, An integrated fluorescence biosensor for microRNA detection based on exponential amplification reaction-triggered three-dimensional bipedal DNA walkers, Anal. Chim. Acta 1143 (2021) 157–165.
[14] M.Q. Ye, Y.J. Kong, C.L. Zhang, Y.F. Lv, S.S. Cheng, D.Y. Hou, Y.Z. Xian, Near-infrared light controllable DNA walker driven by endogenous adenosine triphosphate for in situ spatiotemporal imaging of intracellular microRNA, ACS Nano 15 (2021) 14253–14262.
[15] C. Li, X.X. Li, L.M. Wei, M.Y. Liu, Y.Y. Chen, G.X. Li, Simple electrochemical sensing of attomolar proteins using fabricated complexes with enhanced surface binding avidity, Chem. Sci. 6 (2015) 4311–4317.
[16] L. Li, C.C. Niu, T. Li, Y.F. Wan, Y. Zhou, H.J. Wang, R. Yuan, P. Liao, Ultrasensitive electrochemiluminescence biosensor for detection of laminin based on DNA dendrimer-carried luminophore and DNA nanomachine-mediated target recycling amplification, Biosens. Bioelectron. 101 (2018) 206–212.
[17] X.S. Yang, D.M. Shi, S.M. Zhu, B.J. Wang, X.J. Zhang, G.F. Wang, Portable aptasensor of aflatoxin B1 in bread based on a personal glucose meter and DNA walking machine, ACS Sens. 3 (2018) 1368–1375.
[18] D.Y. Zhang, A.J. Turberfield, B. Yurke, E. Winfree, Engineering entropy-driven reactions and networks catalyzed by DNA, Science 318 (2007) 1121–1125.
[19] Y.F. Lv, L. Cui, R.Z. Peng, Z.L. Zhao, L.P. Qiu, H.P. Chen, C. Jin, X.B. Zhang, W. H. Tan, Entropy beacon: a hairpin-free DNA amplification strategy for efficient detection of nucleic acids, Anal. Chem. 87 (2015) (2015) 11714–11720.
[20] Y.S. Jiang, S. Bhadra, B.L. Li, A.D. Ellington, Mismatches improve the performance of strand-displacement nucleic acid circuits, Angew. Chem. Int. Ed. 53 (2014) 1845–1848.
[21] Y.X. Li, Z.W. Luo, C.Y. Zhang, R. Sun, C. Zhou, C.J. Sun, Entropy driven circuit as an emerging molecular tool for biological sensing: a review, Trac. Trends Anal. Chem. 134 (2021), 116142.
[22] C. Jung, P.B. Allen, A.D. Ellington, A stochastic DNA walker that traverses a microparticle surface, Nat. Nanotechnol. 11 (2016) 157–163.
[23] Y. Cheng, Y.F. Bao, S. Liang, B. Li, Y.L. Liu, H.P. Wu, X.P. Ma, Y.N. Chu, Y. Shao, Q. Meng, G.H. Zhou, Q.X. Song, B.J. Zou, Flap endonuclease 1-assisted DNA walkers for sensitively and specifically sensing ctDNAs, Anal. Chem. 93 (2021) 9593–9601.
[24] M.M. Lv, J.W. Liu, R.Q. Yu, J.H. Jiang, A bipedal DNA nanowalker fueled by catalytic assembly for imaging of base-excision repairing in living cells, Chem. Sci. 11 (2020) 10361–10366.
[25] E.H. Xiong, D.S. Zhen, L. Jiang, X.M. Zhou, Binding-induced 3D-bipedal DNA walker for cascade signal amplification detection of thrombin combined with catalytic hairpin assembly strategy, Anal. Chem. 91 (2019) 15317–15324.
[26] W.W. Qin, L. Chen, Z.R. Wang, Q. Li, C.H. Fan, M.H. Wu, Y.Q. Zhang, Bioinspired DNA nanointerface with anisotropic aptamers for accurate capture of circulating tumor cells, Adv. Sci. 7 (2020), 2000647.
[27] J.F. Yin, S.K. Chen, Y.Y. Song, H.L. Wang, Fluorescent imaging of cytoplasmic nucleolin in live cells by a functionalized-engineered aptamer, Chem. Commun. 56 (2020) 14171–14174.
[28] S. Soundararajan, W.W. Chen, E.K. Spicer, N. Courtenay-Luck, D.J. Fernandes, The nucleolin targeting aptamer AS1411 destabilizes Bcl-2 messenger RNA in human breast cancer cells, Cancer Res. 68 (2008) 2358–2365.
[29] Y. Zheng, X.Y. Wang, S.Q. He, Z.H. Gao, Y. Di, K.L. Lu, K. Li, J.D. Wang, Aptamer-DNA concatamer-quantum dots based electrochemical biosensing strategy for green and ultrasensitive detection of tumor cells via mercury-free anodic stripping voltammetry, Biosens. Bioelectron. 126 (2019) 261–268.
[30] J.D. Wang, X.Y. Wang, H.S. Tang, S.Q. He, Z.H. Gao, R.X. Niu, Y. Zheng, S.M. Han, A ratiometric magnesium sensor using DNAzyme-templated CdTe quantum dots and Cy5, Sensor. Actuator. B Chem. 272 (2018) 146–150.
[31] T. Zhang, T.R. Tian, R.H. Zhou, S.H. Li, W.J. Ma, Y.X. Zhang, N.X. Liu, S.R. Shi, Q. S. Li, X.P. Xie, Y.C. Ge, M.T. Liu, Q. Zhang, S.Y. Lin, X.X. Cai, Y.F. Lin, Design, fabrication and applications of tetrahedral DNA nanostructure-based multifunctional complexes in drug delivery and biomedical treatment, Nat. Protoc. 15 (2020) 2728–2757.
[32] J.J. Li, X.Q. Zhong, F.F. Cheng, J.R. Zhang, L.P. Jiang, J.J. Zhu, One-pot synthesis of aptamer-functionalized silver nanoclusters for cell-type-specific imaging, Anal. Chem. 84 (2012) 4140–4146.
[33] F.J. Huang, M.H. Lin, R.L. Duan, X.D. Lou, F. Xia, I. Willner, Photoactivated specific mRNA detection in single living cells by coupling "signal-on" fluorescence and "signal-off" electrochemical signals, Nano Lett. 18 (2018) 5116–5123.